HHS Public Access

Author manuscript

ACS Macro Lett. Author manuscript; available in PMC 2017 May 17.

Published in final edited form as:

ACS Macro Lett. 2015 October 20; 4(10): 1081–1084. doi:10.1021/acsmacrolett.5b00545.

Anti-tumor Efficacy Study using Irreversible Electroporation and Doxorubicin-loaded Polymeric Micelles

Jun Zhao[1], **John Qiao**[2], **Min Zhou**[1], **Sanjay Gupta**[2], **Chun Li**[1,*], and **Marites P. Melancon**[2,*]

[1]Department of Cancer Systems Imaging, The University of Texas MD Anderson Cancer Center, 1515 Holcombe Blvd., Houston, TX 77030

[2]Department of Interventional Radiology, The University of Texas MD Anderson Cancer Center, 1515 Holcombe Blvd., Houston, TX 77030

Abstract

Irreversible electroporation (IRE) is a novel non-thermal ablative treatment for cancer patients with unresectable tumor. IRE kills tumor cells by applying a strong electric field across the cell membrane, thereby creating irreparable pores. Compared to conventional thermal ablation, IRE is effective in perivascular tissues and can preserve the surrounding sensitive structures. However, tumor cells may survive in the regions exposed to insufficient electric field strength, and cause tumor relapse afterwards. We prepared a doxorubicin-loaded polymeric micelles system (M-Dox) using oil-in-water emulsion. The resultant M-Dox was 37.9 ± 3.2 nm in size with a Dox loading of 4.3% by weight. M-Dox is toxic to multiple human cancer cell lines with IC_{50} values in nanomolar and micromolar range. When combined with IRE in a hepatic carcinoma mouse xenograft model, the tumor treated with the combination therapy (IRE + M-Dox) was the highest in both M-Dox uptake and percentage of necrosis. Immunohistochemical staining also confirmed that the fewest proliferating cells were present after the combination therapy. Our data suggested that M-Dox was an effective adjuvant treatment to enhance the anti-tumor efficacy of IRE.

Keywords

Irreversible Electroporation; Micelles; Doxorubicin; Hepatocellular carcinoma

Despite the improvement in the early diagnosis of cancer, many patients are poor candidates for surgical resection of tumor due to the stage and/or location of diseases[1]. For this cohort of patients with unresectable tumor, minimally invasive therapies are important alternatives to ablate tumor locally. The commonly used ablative techniques include percutaneous ethanol injection, radiofrequency, microwave, laser-induced interstitial thermal therapy, high-intensity focused ultrasound, and cryoablation[2]. So far, most ablative techniques kill tumor cells by inducing significant temperature change within the ablation zone. However,

*Corresponding Author: Chun Li, PhD, Department of Cancer Systems Imaging, The University of Texas MD Anderson Cancer Center, cli@mdanderson.org; Marites P. Melancon, PhD, Department of Interventional Radiology, The University of Texas MD Anderson Cancer Center, mmelancon@mdanderson.org.

ASSOCIATED CONTENT

Detailed experimental procedures are described in supporting information. This material is available free of charge via the Internet at http://pubs.acs.org.

the treatment response is often complicated by the collateral damage to the nearby ducts or blood vessels. In the meantime, the efficacy of thermal ablation can be limited by the “heat sink” effect, when the blood flow in the adjacent vasculatures could dissipate the thermal energy, causing suboptimal ablation and eventually tumor recurrence[3].

Recently, irreversible electroporation (IRE) has proven useful in treating patients with perivascular tumors[4]. Instead of causing temperature change, IRE kills tumor cells by creating irreparable pores on cell membrane[5]. The persistent leakage of cell membrane soon leads to the loss of endocytic homeostasis and consequently cell death[6]. IRE exhibits many advantages over the conventional thermal ablation. First, IRE only affects the membrane of cells, sparing most of the other tissue molecules. IRE remains effective near blood vessels, and the whole treatment can be administered in as short as several minutes[7]. Importantly, IRE could preserve the nearby sensitive structures such as urethera and myelin sheaths[8]; and leave the extracellular matrix and major tissue vasculature largely intact. Notably, IRE usually forms a minimal scar that can dissolute in several weeks after the treatment. The rapidly absorbed scar will not interfere with the post-treatment diagnosis of residual or recurrent tumors[9].

The cell-killing efficacy of IRE depends on the electric field strength (E), to which the cells are exposed locally. If E drops below a certain threshold when the cell membrane could recover following the offset of electric pulses, the effect is called reversible electroporation (RE). Although it has been used extensively to transport molecules or nanoparticles across the cell membrane[10], RE does not kill tumor cell by itself. As a result, the tumor cells exposed to insufficient electric field strength, i.e. RE, may survive the treatment and cause tumor recurrence afterwards. The number of these residual tumor cells can be minimized by using IRE probes with advanced array geometry along with mathematical simulation of the distribution of intratumoral E[11]. However, due to the irregular geometry and heterogeneity of tumor mass, it is unlikely to achieve a uniform IRE-induced killing throughout the tumor mass. On the other hand, chemotherapy drugs have been used in combination with RE. One of the most commonly used drug is bleomycin[12]. In this study, we prepared a doxorubicin-loaded micelles system (M-Dox) and evaluated its efficacy in combination with IRE. We hypothesize that the combination of IRE and M-Dox has better anti-tumor efficacy than IRE alone.

M-Dox was prepared via the oil-in-water emulsion method using a crosslinkable block copolymer as the macromolecular surfactant (Figure 1A). ^{1}H-NMR spectrum revealed that each copolymer was constituted of 10 units of MAPEG (hydrophilic block) and 20 units of MESPS (hydrophobic block). The resultant M-Dox (Figure 1C) was 37.9 ± 3.2 nm in size (polydispersity index or PDI 0.145) with a doxorubicin loading of 4.3 % by weight. TEM micrograph confirmed that M-Dox had spherical morphology with diameters between 50 to 100 nm (Figure 1D). The slightly larger micelles size from TEM may be attributed to the particle deformation during the preparation of TEM samples. Due to the acid-induced degradation of PLGA, doxorubicin was released from M-Dox at 37 °C in a pH-dependent manner (Figure 1E). The release was faster at pH 5.2 than at pH 7.4. Up to 60% of drug was released at pH 5.2 after 7 days of incubation, at which time less than 10% was released at pH 7.4. Notably, the size of M-Dox did not change dramatically during degradation,

probably because of crosslinking silane. After 7 days of incubation at 37 C, the size decreased from 37.9 ± 3.2 at day 0 to 25.2 ± 2.5 at day 7; while the PDI increased from 0.145 to 0.308.

We first studied the effect of M-Dox on cell proliferation in four cancer cell lines (Figure S1): U87 (human glioblastoma), HeLa (human cervical cancer), Miapaca-2 (human pancreatic adenocarcinoma), and Hep3B (human hepatocellular carcinoma). Cell viability was measured after 96 hrs of co-incubation with free Dox or M-Dox. Both Dox and M-Dox showed excellent anti-proliferation efficacy, while M-Dox was less toxic than free Dox. The anti-proliferation IC_{50} values for Dox and M-Dox (nM) were: 77.5 ± 8.9 vs. 444.9 ± 33.5 for U87, 17.1 ± 2.5 vs. 51.8 ± 6.1 for HeLa, 0.97 ± 0.07 vs. 30.7 ± 2.6 for Miapaca-2, and 30.5 ± 2.5 vs. 92.1 ± 8.0 for Hep3B.

The effect of electroporation field strength (V/cm) on Hep3B cell viability was then tested (Figure 2A). No significant cell death was observed up to 500 V/cm, above which the cell viability decreased as the field strength increased. Therefore, 500 V/cm was chosen for reversible electroporation and 2500 V/cm for irreversible electroporation. For *in vitro* combination therapy, Hep3B cells were treated with 50 μM M-Dox along with reversible electroporation (RE) at 500 V/cm. Non-treatment cells and monotherapy groups were used as control. Figure 2B shows that the combination group had significant lower cell viability than either monotherapy groups ($p < 0.05$).

The in vivo effects of the combination therapy were investigated using Hep3B subcutaneous xenograft model. Tumors were collected 24 hrs after treatment and sectioned for the analyses in M-Dox uptake, necrosis and cell proliferation. The results of M-Dox uptake are summarized in Figure 3. Compared to M-Dox monotherapy, both RE + M-Dox and IRE + M-Dox increased the number of M-Dox-positive nuclei by 1.7 and 2.7 folds, respectively ($p < 0.05$). Representative tumor necrosis from H&E stained tumor tissues are presented in Figure 4. The percentage of necrosis (%) in IRE + M-Dox treated tumor (97.2 ± 0.5%) was significantly higher than those of tumors treated by IRE (86.5 ± 0.5%) or M-Dox (46.7 ± 9.1%) ($p < 0.05$). There were no significant difference among the RE, M-Dox and RE + M-Dox groups. The cell proliferation of treated tumors are shown in Figure 5. Among the monotherapy groups, the IRE groups had the fewest proliferating cells than either RE or M-Dox group ($p < 0.05$). For combination therapies, the IRE + M-Dox group had fewer proliferating cells than either IRE or M-Dox group ($p < 0.05$).

In this study, we successfully prepared a novel doxorubicin-loaded polymeric micelles system via oil-in-water emulsion using an *in situ* crosslinkable amphiphilic polymeric stabilizer. The resultant M-Dox showed excellent toxicity to different types of human cancer cells. The combination therapy of IRE and M-Dox showed the best anti-tumor efficacy in Hep3B xenograft model compared to the monotherapy groups.

Oil-in-water emulsion is widely used to prepare nanoparticles loaded with hydrophobic chemotherapy drugs[13]. An important step during the emulsion is to form a stable dispersion of micrometric oil droplet stabilized by small-molecular or macromolecular surfactants[14]. During the post-emulsion evaporation, the organic solvent inside the oil droplets evaporates,

and the micro-droplets solidify into nanoparticles coated by the surfactants. However, since most surfactants are not covalently bound to the nanoparticles, the stability of nanoparticle may be insufficient. We hereby developed a novel amphiphilic polymeric surfactant, PEG-*b*-poly(MESPS), which can crosslink *in situ* through the hydrolysis of silane groups. As a result, the PLGA/Dox core were covered by a mesh network of crosslinked PEG-b-poly(MESPS) (Figure 1C). The ammonium functionality at the exterior termini of PEG block (Figure 1A) could be used to conjugate with targeting ligands or diagnostic imaging tracers[13b]. Due to the crosslinked silane, M-Dox showed excellent size stability (Figure 1F) and retained most of Dox at physiological pH up to 1 week (Figure 1E). Dox was quickly released in acidic environment, which is an advantage since tumor microenvironment is typically acidic[15]. The anti-tumor efficacy of M-Dox was validated in four human cancer cell lines, with IC_{50} values (Figure S1) at nanomolar to micromolar ranges. M-Dox was less toxic than free Dox, because of the controlled release of Dox during the incubation.

Various nanoparticles have been used to enhance thermal ablation[16]. For example, high-intensity focused ultrasound (HIFU) is used to stimulate the intratumoral release of drugs from liposomes[17], or to locally vaporize perfluorocarbons in micro/nano-bubbles to generate high-resolution ultrasound imaging[18]. Inorganic nanoparticles, e.g. gold nanoparticles and single-wall carbon nanotubes, could generate heat in the presence of radiofrequency (RF), microwave (MW), or near infrared (NIR) laser irradiation[19]. In consequence, the effective area of thermal ablation can be increased[16]. The tumor-specific localization of such nanoparticles can also focus the thermal energy to the tumor region and minimize collateral damage to the nearby tissues. Mouli, et al has recently published on the use of SPIO-loaded with doxorubicin in combination with IRE to increase the accumulation of drug-carrying nanoparticle in N1S1 rat hepatoma and VX2 rabbit tumor models[20]. Although the authors showed increased accumulation into the target tissues, treatment efficacy was not presented. To our best knowledge, this manuscript presented the first example to combine IRE with activatable chemodrug-loaded nanoparticles with acute treatment efficacy. Unlike thermal ablation, IRE selectively disrupts cell membranes and enables the intracellular delivery of nanoparticles[21]. As shown in Figure 3, more cell nuclei expressed the fluorescence of Dox after IRE or RE. M-Dox was directly injected into tumor so that each tumor was exposed to the same dose of M-Dox. Without electroporation, the intratumoral distribution of M-Dox was uneven (Figure 3B), which is in accordance with previous reports about the limitations of intratumoral injection. In the meantime, electroporation increased the intracellular delivery of M-Dox, whereas IRE was more potent than RE (Figure 3D vs. C), probably because IRE could better permeate cell membranes.

For the anti-tumor efficacy studies, we first tested *in vitro* whether M-Dox could improve cell killing under the condition of reversible electroporation. A field strength of 500 V/cm was chosen for RE since it did not affect cell viability (Figure 2A). When M-Dox (50 μM) was added during the electroporation (Figure 2B), the combination group (RE + M-Dox) yielded lower cell viability than either RE or M-Dox alone. We further evaluated the anti-tumor efficacy of M-Dox in combination with electroporation in a Hep3B xenograft model. Treating tumor with electroporation and M-Dox caused acute tumor necrosis (Figure 4). IRE + M-Dox caused the highest percentage of necrosis among all the treatment groups. The

necrosis data correlated with the immunohistochemical staining for cell proliferation (Figure 5), where the IRE + M-Dox treated tumor had the fewest proliferating cells ($Ki67^+$).

The current study was limited that only acute tumor response was analyzed, and the M-Dox was intratumorally injected. A long-term monitoring of tumor growth and animal survival will be conducted to fully understand the anti-tumor efficacy of the combination therapy. In order to further improve the intratumoral distribution of nanoparticles, M-Dox will be intravenously injected in future. The uptake of M-Dox in tumor and other organs will be measured by biodistribution study.

In summary, we successfully prepared doxorubicin-loaded micelles via a novel oil-in-water emulsion technique. We showed that the combination therapy of electroporation and M-Dox was an effective treatment against multiple cultured cell lines, as well as in a human hepatic carcinoma xenograft model. While the IRE treatment killed most of tumor cells, the adjuvant treatment with M-Dox further increase the percentage of tumor necrosis, and depleted the fraction of proliferating tumor cells. Further studies are warranted to evaluate animal survival during treatment. A systemic administration of chemodrug-loaded nanoparticles will also be used.

Supplementary Material

Refer to Web version on PubMed Central for supplementary material.

Acknowledgments

Funding Sources

Any funds used to support the research of the manuscript should be placed here (per journal style).

References

1. Wyld L, Audisio RA, Poston GJ. The evolution of cancer surgery and future perspectives. Nat Rev Clin Oncol. 2015; 12(2):115–24. [PubMed: 25384943]
2. Li D, Kang J, Golas BJ, Yeung VW, Madoff DC. Minimally invasive local therapies for liver cancer. Cancer Biol Med. 2014; 11(4):217–36. [PubMed: 25610708]
3. Mulier S, Ni Y, Jamart J, Ruers T, Marchal G, Michel L. Local recurrence after hepatic radiofrequency coagulation: multivariate meta-analysis and review of contributing factors. Ann Surg. 2005; 242(2):158–71. [PubMed: 16041205]
4. Charpentier KP, Wolf F, Noble L, Winn B, Resnick M, Dupuy DE. Irreversible electroporation of the liver and liver hilum in swine. HPB (Oxford). 2011; 13(3):168–73. [PubMed: 21309933]
5. Davalos RV, Mir IL, Rubinsky B. Tissue ablation with irreversible electroporation. Ann Biomed Eng. 2005; 33(2):223–31. [PubMed: 15771276]
6. Guo Y, Zhang Y, Klein R, Nijm GM, Sahakian AV, Omary RA, Yang GY, Larson AC. Irreversible Electroporation Therapy in the Liver: Longitudinal Efficacy Studies in a Rat Model of Hepatocellular Carcinoma. Cancer Research. 2010; 70(4):1555–1563. [PubMed: 20124486]
7. Cannon R, Ellis S, Hayes D, Narayanan G, Martin RC 2nd. Safety and early efficacy of irreversible electroporation for hepatic tumors in proximity to vital structures. J Surg Oncol. 2012
8. Neal RE, Davalos RV. The Feasibility of Irreversible Electroporation for the Treatment of Breast Cancer and Other Heterogeneous Systems. Annals of Biomedical Engineering. 2009; 37(12):2615–2625. [PubMed: 19757056]

9. Rubinsky B, Onik G, Mikus P. Irreversible electroporation: a new ablation modality–clinical implications. Technol Cancer Res Treat. 2007; 6(1):37–48. [PubMed: 17241099]
10. (a) Yamashita YI, Shimada M, Hasegawa H, Minagawa R, Rikimaru T, Hamatsu T, Tanaka S, Shirabe K, Miyazaki JI, Sugimachi K. Electroporation-mediated interleukin-12 gene therapy for hepatocellular carcinoma in the mice model. Cancer Res. 2001; 61(3):1005–12. [PubMed: 11221826] (b) Granot Y, Rubinsky B. Mass transfer model for drug delivery in tissue cells with reversible electroporation. International Journal of Heat and Mass Transfer. 2008; 51(23–24): 5610–5616. [PubMed: 19884974]
11. (a) Arena CB, Sano MB, Rylander MN, Davalos RV. Theoretical considerations of tissue electroporation with high-frequency bipolar pulses. IEEE Trans Biomed Eng. 2011; 58(5):1474–82. [PubMed: 21189230] (b) Gowrishankar TR, Esser AT, Smith KC, Son RS, Weaver JC. Intracellular electroporation site distributions: modeling examples for nsPEF and IRE pulse waveforms. Conf Proc IEEE Eng Med Biol Soc. 2011; 2011:732–5. [PubMed: 22254414]
12. Jaroszeski MJ, Gilbert RA, Heller R. In vivo antitumor effects of electrochemotherapy in a hepatoma model. Biochim Biophys Acta. 1997; 1334(1):15–8. [PubMed: 9042359]
13. (a) Tadros T, Izquierdo P, Esquena J, Solans C. Formation and stability of nano-emulsions. Adv Colloid Interface Sci. 2004; 108–109:303–18.(b) Gianella A, Jarzyna PA, Mani V, Ramachandran S, Calcagno C, Tang J, Kann B, Dijk WJ, Thijssen VL, Griffioen AW, Storm G, Fayad ZA, Mulder WJ. Multifunctional nanoemulsion platform for imaging guided therapy evaluated in experimental cancer. ACS Nano. 2011; 5(6):4422–33. [PubMed: 21557611]
14. Choudhury H, Gorain B, Karmakar S, Biswas E, Dey G, Barik R, Mandal M, Pal TK. Improvement of cellular uptake, in vitro antitumor activity and sustained release profile with increased bioavailability from a nanoemulsion platform. Int J Pharm. 2014; 460(1–2):131–43. [PubMed: 24239580]
15. Wang L, Fan Z, Zhang J, Changyi Y, Huang C, Gu Y, Xu Z, Tang Z, Lu W, Wei X, Li C. Evaluating tumor metastatic potential by imaging intratumoral acidosis via pH-activatable near-infrared fluorescent probe. Int J Cancer. 2015; 136(4):E107–16. [PubMed: 25155456]
16. Manthe RL, Foy SP, Krishnamurthy N, Sharma B, Labhasetwar V. Tumor ablation and nanotechnology. Mol Pharm. 2010; 7(6):1880–98. [PubMed: 20866097]
17. Oerlemans C, Deckers R, Storm G, Hennink WE, Nijsen JF. Evidence for a new mechanism behind HIFU-triggered release from liposomes. J Control Release. 2013; 168(3):327–33. [PubMed: 23567041]
18. Huang HY, Hu SH, Hung SY, Chiang CS, Liu HL, Chiu TL, Lai HY, Chen YY, Chen SY. SPIO nanoparticle-stabilized PAA-F127 thermosensitive nanobubbles with MR/US dual-modality imaging and HIFU-triggered drug release for magnetically guided in vivo tumor therapy. J Control Release. 2013; 172(1):118–27. [PubMed: 23933522]
19. (a) Rejinold NS, Jayakumar R, Kim YC. Radio frequency responsive nano-biomaterials for cancer therapy. J Control Release. 2015; 204:85–97. [PubMed: 25744825] (b) You J, Zhang G, Li C. Exceptionally high payload of doxorubicin in hollow gold nanospheres for near-infrared light-triggered drug release. ACS Nano. 2010; 4(2):1033–41. [PubMed: 20121065]
20. Mouli SK, Tyler P, McDevitt JL, Eifler AC, Guo Y, Nicolai J, Lewandowski RJ, Li W, Procissi D, Ryu RK, Wang YA, Salem R, Larson AC, Omary RA. Image-guided local delivery strategies enhance therapeutic nanoparticle uptake in solid tumors. ACS Nano. 2013; 7(9):7724–33. [PubMed: 23952712]
21. Jaroszeski MJ, Gilbert R, Nicolau C, Heller R. Delivery of genes in vivo using pulsed electric fields. Methods Mol Med. 2000; 37:173–86. [PubMed: 21445735]

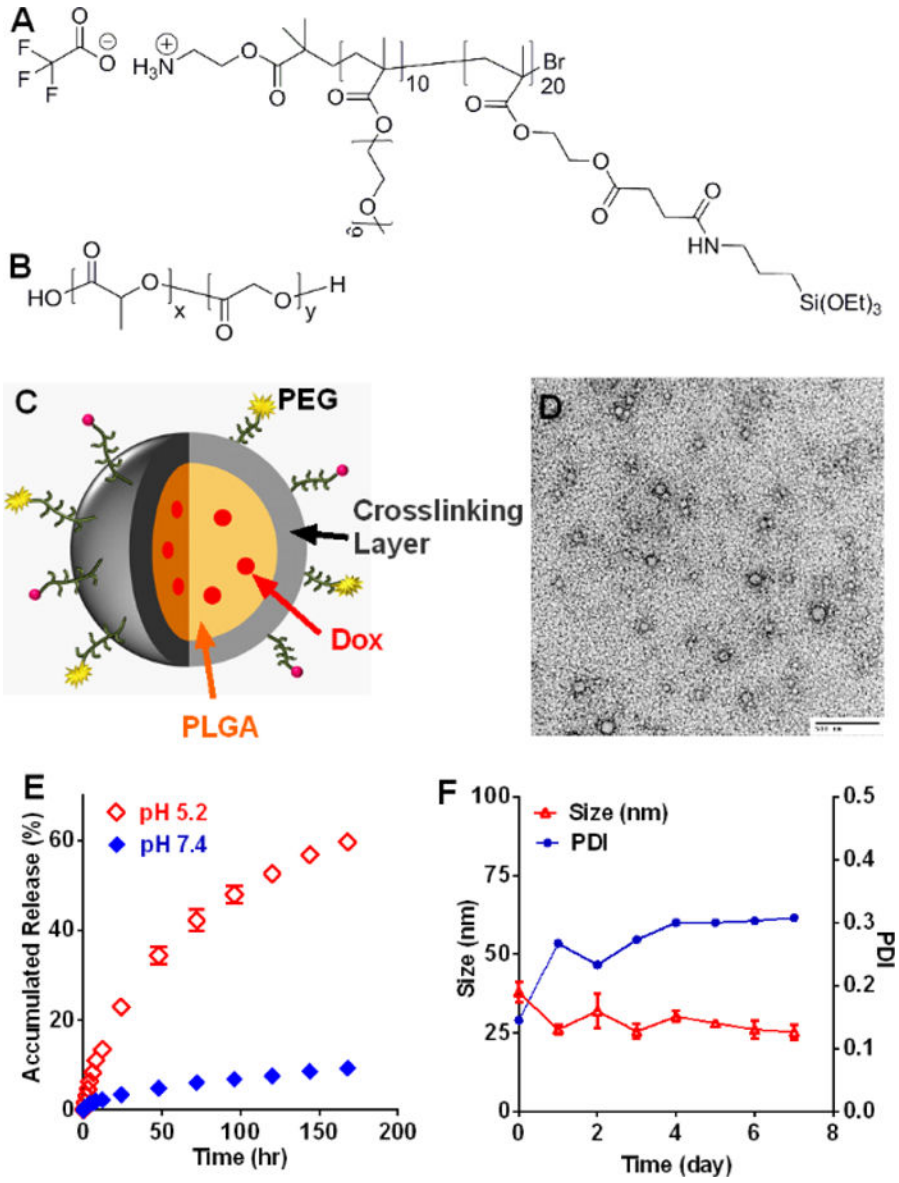

Figure 1.

Preparation and characterization of doxorubicin-loaded micelles (M-Dox). Chemical structure of (A) crosslinkable block copolymer and (B) poly(lactic-co-glycolic acid), PLGA. (C) Schematic illustration of M-Dox. (D) TEM micrograph of M-Dox (scale bar = 500 nm). (E) Doxorubicin release profile at 37 °C. (F) Hydrodynamic size and polydiversity index (PDI) of M-Dox during degradation at 37 °C.

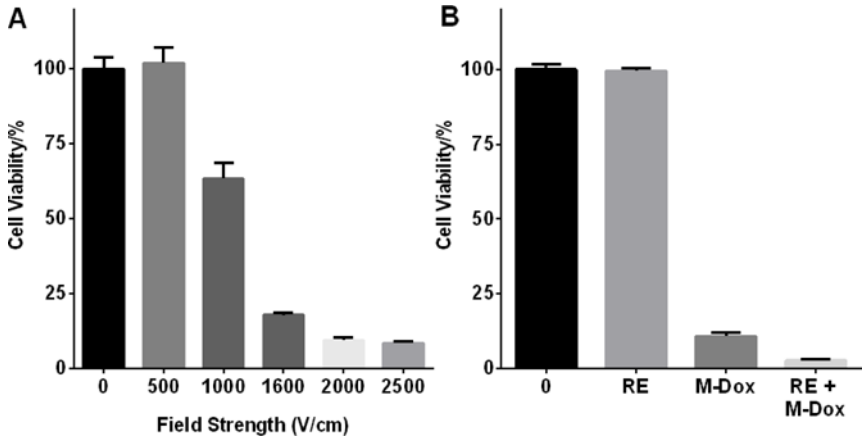

Figure 2.

Effect of M-Dox and electroporation treatment on Hep3B viability. (A) Hep3B viability after electroporation at different field strength. (B) Hep3B viability after treatment with M-Dox, reversible electroporation (RE, 500 V/cm), and combination of RE + M-Dox. The combination group had the lowest cell viability among all four groups ($p < 0.05$).

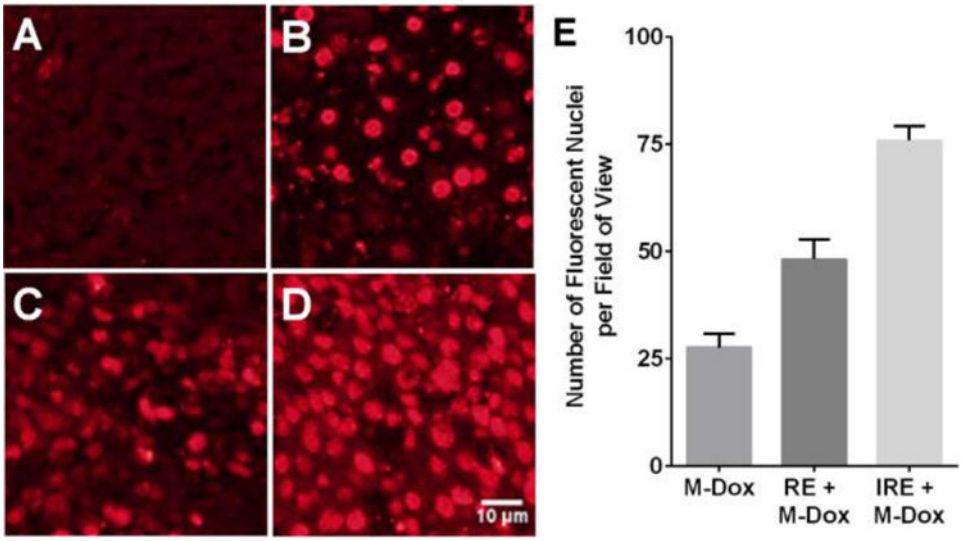

Figure 3.

In vivo uptake of M-Dox in the presence of electroporation. (A) Non-treatment control, (B) M-Dox, (C) RE + M-Dox, (D) IRE + M-Dox. The quantitative results are summarized in panel E. Data points were presented as mean ± standard error of mean (N = 9). Each group was significantly different from the others ($p < 0.05$)

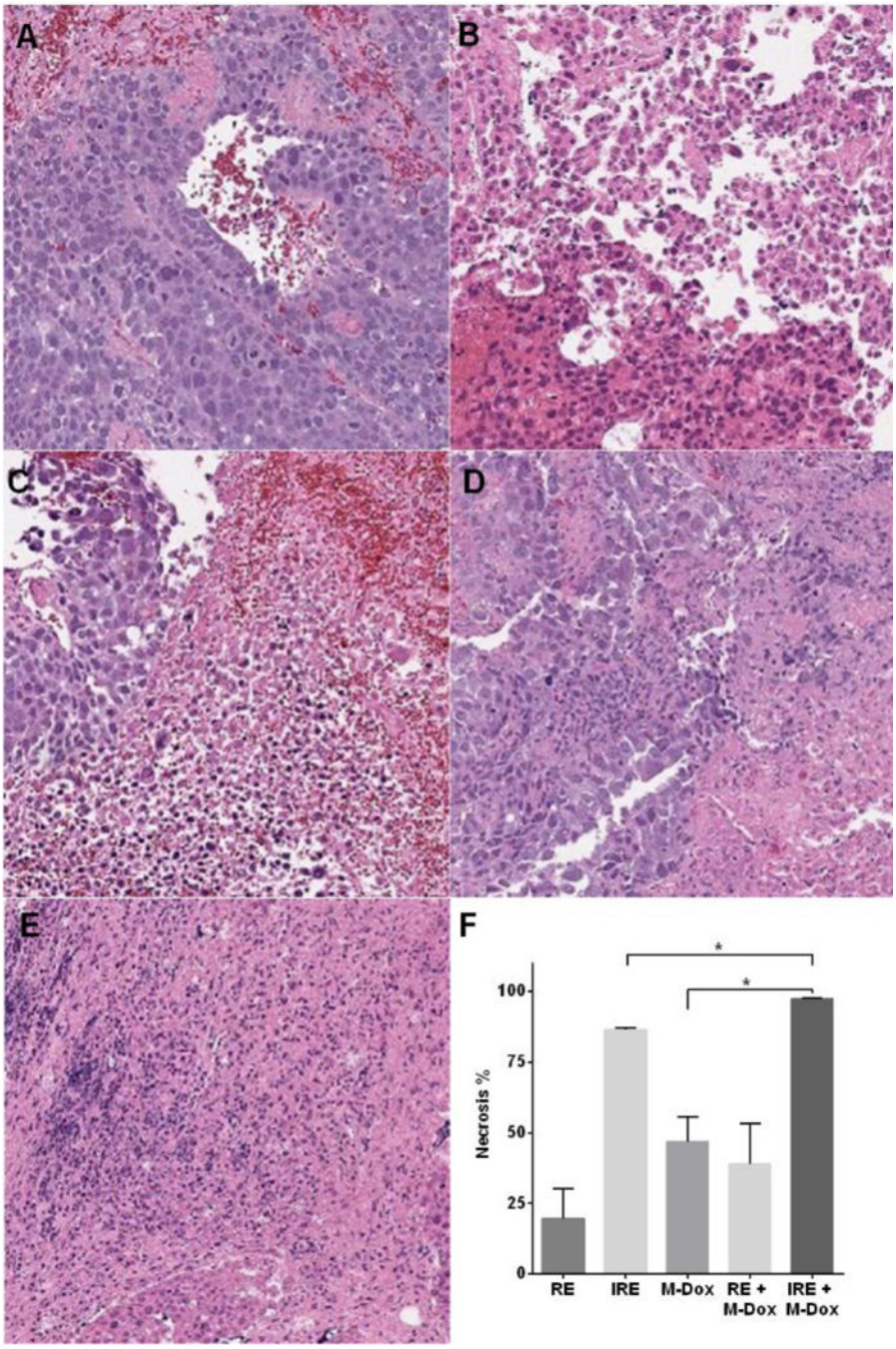

Figure 4.

H&E Analyses of treated tumors and quantification of necrosis. (A) RE, (B) IRE, (C) M-Dox, (D) RE + M-Dox, and (E) IRE + M-Dox. The quantitative results are summarized in panel F. Data points were presented as mean ± standard error of mean (N = 3).

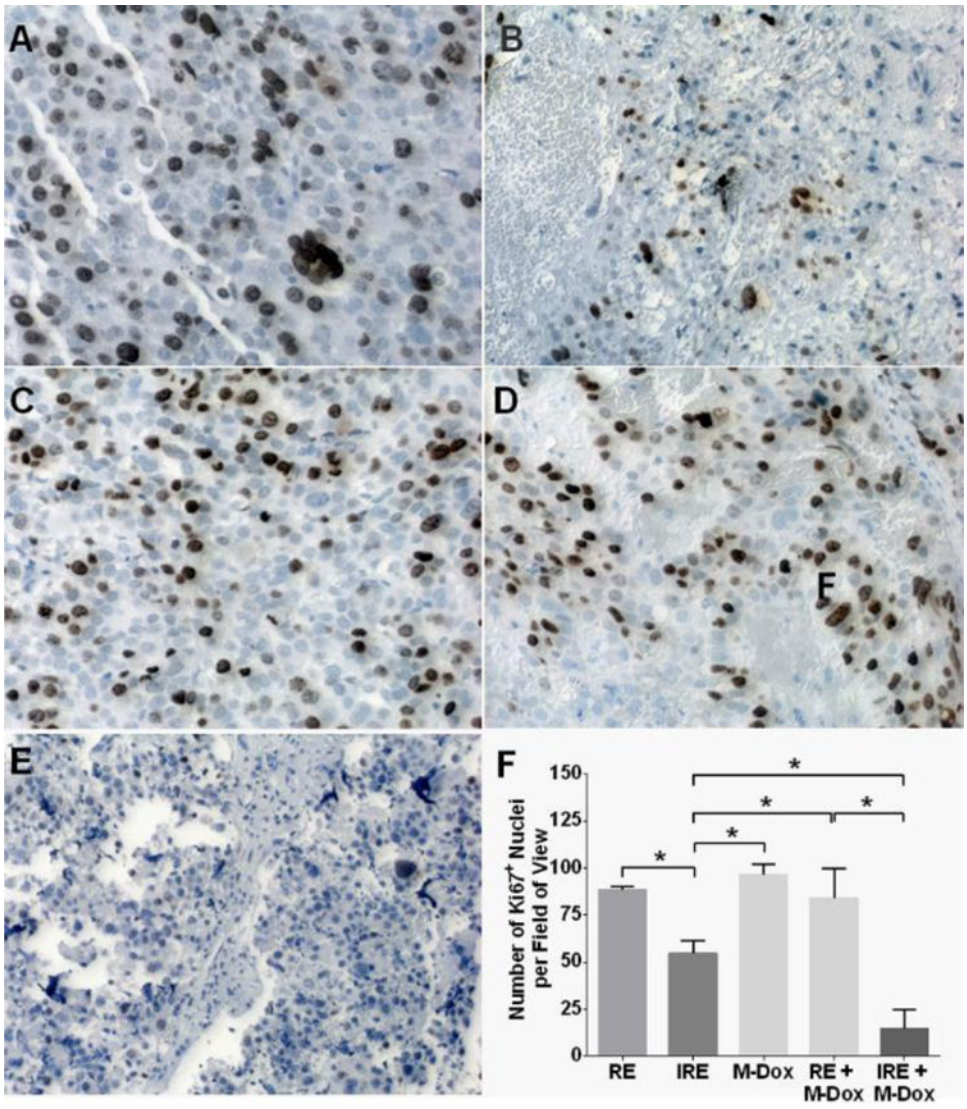

Figure 5.

Immunohistochemical staining for proliferating cells ($Ki67^+$) on sections of treated tumors. Representative micrographs are shown in panels A–E: (A) RE, (B) IRE, (C) M-Dox, (D) RE + M-Dox, and (E) IRE + M-Dox. The quantitative results are summarized in panel F. Data was generated from at least 10 randomly chosen field-of-views in each treatment group. Significant differences are marked with * ($p < 0.05$).